Atmospheric-pressure plasma actuators: Enhancement of the free charges' transport mechanism

Atmospheric pressure plasma actuators: enhancement of the free charges transport mechanism

A.C. Ricchiuto[1], C.A. Borghi[1], A. Cristofolini[1], and G. Neretti[1]

[1] Department of Electrical, Electronic, and Information Engineering, University of Bologna, Italy

Abstract

Charge particles can increase the biocidal efficacy of non-thermal plasmas in indirect treatments. The aim of this work is to increase the amount of free charges produced and delivered by a Surface Dielectric Barrier Discharge fluid-dynamics actuator. Different linear actuators and supplying conditions have been considered. Actuators were utilized to produce an ionic wind impinging an insulating target surface. Charged particles distribution over the target was measured with and without a metallic mesh between actuator and target itself. Linear actuators have proven to be more effective in charge delivery with respect an annular one previously studied by our research team. A 2D electrostatic finite element analysis has been carried out to get a better insight of this physical behavior.

1. Introduction

Plasma Synthetic Jet Actuator (PSJA) realized by means of a Surface Dielectric Barrier Discharge (SDBD) device produces an ionic wind perpendicular to the surface of the actuator itself [1]. This effect is obtained through a peculiar geometry of the SDBD as shown by several authors [2][3][4]. As a result of it the induced jet perpendicular to the SDBD surface is obtained through the Electro Hydro Dynamic (EHD) interaction of the SDBD discharge [5] [6]. The jets propagate for some centimetres at a velocity of some meters per seconds [2]. When PSJA is utilized for indirect treatments in biology, the surface of pathogens or cells near the ionic wind react with oxygen and nitrogen species (RNOS), and a significant amount of charged particles produced by the plasma [7][8]. The charge particles contribution in indirect sterilization treatments had long been ignored. At our knowledge, just few research groups investigated this phenomena [9]-[10]. In these works, the treatment is indirect, but the plasma is still very close to the sample (few millimetres). On the contrary, the directional thrust of PSJA allows charges to reach the sample, positioned at several centimetres from the plasma source. As a matter of fact, free charged particles and other reactive species reach the target mostly for the advection due to the EHD effect [11][12][13]. These charges are always positive. A possible candidate is H_3O^+ ion, that is produced in relatively high amount in air discharges even if humidity degree is quite low [14]. PSJA can operate in ambient air at atmospheric pressure. For this reason and due to its flexibility and low costs, it can be utilized for different applications [16] [15]. In the last years the DBD plasma discharges have been utilized for the decontamination in aqueous solutions [17] [18], for bacteria inactivation and sterilization [19] [18] [21] and other chemical reactions [22].

In a previous work, we experimentally pointed out the contribution of the charge particles of DBD air plasmas in *Candida Guillermondi* indirect inactivation [23]. In all tests, treated sample was positioned at a 2 cm distance from plasma surface. The results showed that an additional Log 1 CFU (Colony-Forming Unit) reduction was achieved when the free charges produced by the PSJA could reach the sample. Therefore, the factors which contribute to the charged particles production and diffusion, have been investigated. In Ref. [24] the role of air humidity in the charges produced by a PSJA was studied. It was observed that transported charged particles can be incremented by increasing electric field and decreasing humidity, by living unchanged both discharge average power and EDH induced jet.

In the present investigation, in order to increase charge delivery process, actuator geometry has been varied. Two linear SDBD actuators had been studied. An actuator was made with a PVC dielectric between the electrodes. The other one was built with a thicker dielectric slab made of Teflon. In linear actuators the induced jet propagates tangentially to actuator surface hitting the target placed perpendicular to the jet. In this way, the merging of the tangential jets occurring in the PSJA configuration is avoided, and the recombination of the charged particles produced in the plasma is reduced. By following experiments carried out in a previous work [23], a metal wire mesh between the actuator and the target had been added. The presence of the mesh was utilized to verify the possibility to prevent charged particles to reach the sample. The mesh had been grounded or left floating. The potential and its distribution on the target surface had been measured and the charge amount had been determined. A 2D finite element analysis, which utilises as inputs the measured quantities, had been carried out to investigate the mechanisms of the charge particle transport.

2. Materials and methods

The configuration of SDBD actuator used in this investigation was a linear one. PVC and Teflon were used as dielectric materials. The former was utilized because it was the same material used in previous studies [12] [23]. This choice helps in the comparison between present and previous results. Teflon was utilized because it is more resistant to thermal effects produced by the surface discharge. In the following the PVC linear actuator will be named Actuator 1. The Teflon linear actuator will be named Actuator 2. Both actuators consist of an asymmetric electrode pair separated by a dielectric slab (see Figure 1), with 35 μm thick linear copper electrodes. The width of the high voltage electrode (HV) was 5 mm. The width of the grounded electrode (GND) was 12 mm (x-direction in Figure 1). The spanwise length of both (in z-direction in Figure 1) was 50 mm. In the first series of tests a PVC dielectric slab with a 2 mm thickness ('T' quotation in Figure 1) was used. For actuator 2 was 'T' was set to 6 mm. The length of plasma discharge ('P' in the Figure 1) is 5 mm for Actuator 1 and 8 mm for Actuator 2. The distance from the end of the plasma discharge to the end of the dielectric slab is about 10 mm for both actuators. The induced flow due to the EHD interaction is produced in the positive x direction (Figure 1).

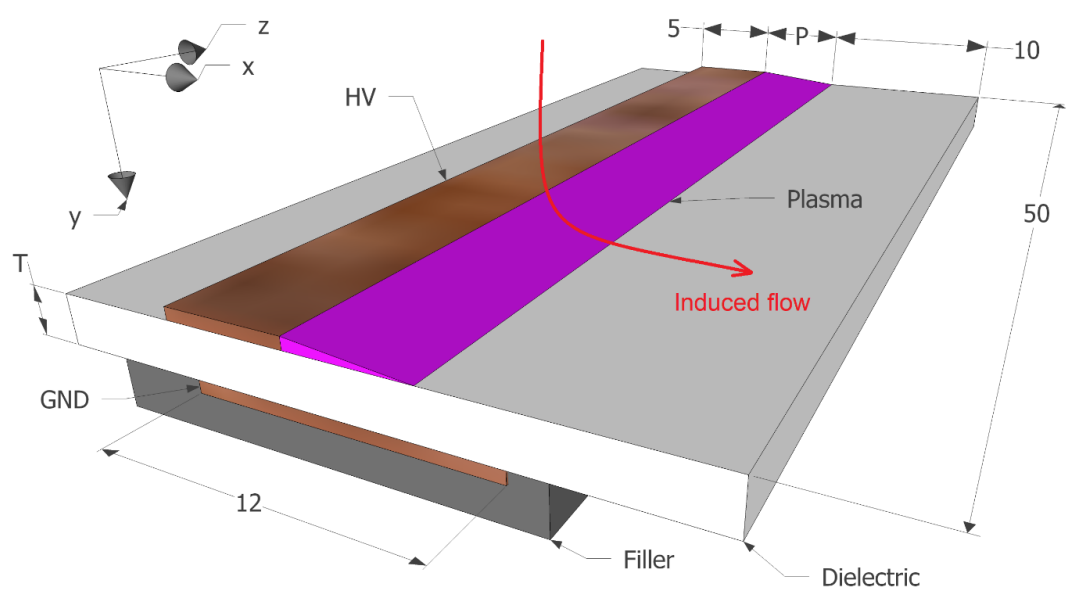

Figure 1. *The SDBD plasma actuator with the dissymmetric electrode pair separated by a dielectric slab.*

A third actuator, namely the PVC annular actuator described in [12], will be named Actuator 3. This octagonal PSJA has a side length of 12 mm, and it will be utilized as reference actuator for both velocity profiles and induced potential distributions produced by deposited charges. A sketch of this actuator is displayed in Figure 2.

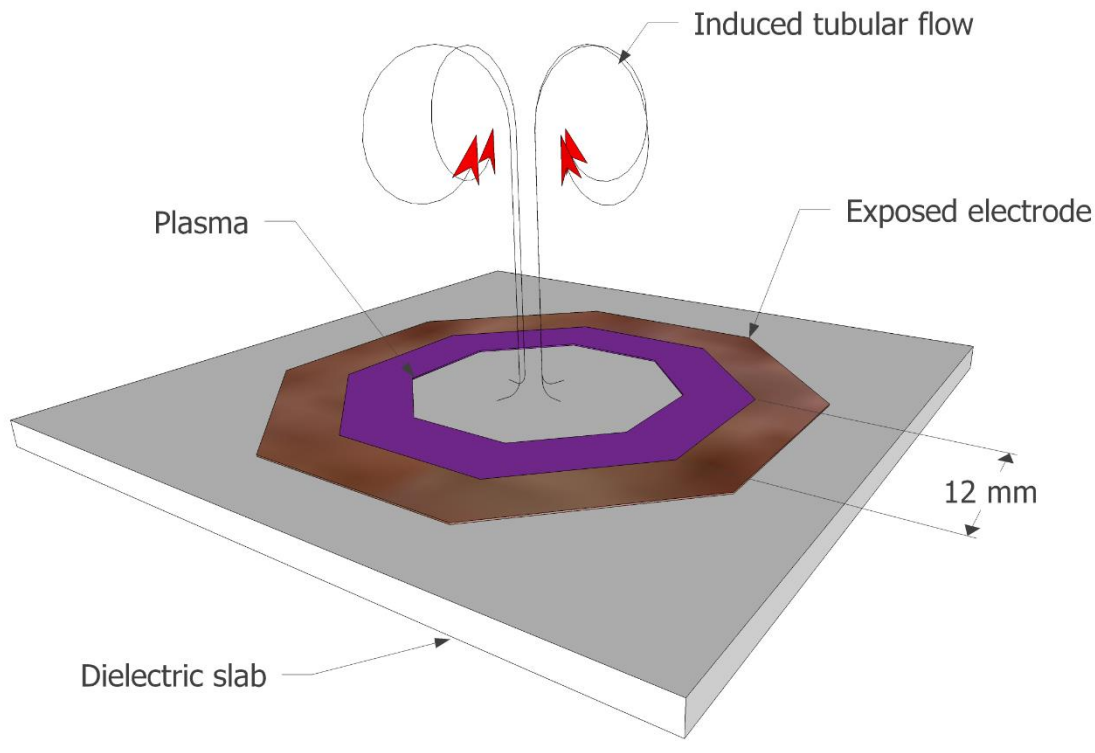

Figure 2. *Sketch of Actuator 3 utilized as reference actuator.*

A sinusoidal supply system, constituted by a push–pull high voltage transformer controlled by an Arduino has been utilized to feed the discharge [25]. It allows to change both voltage and frequency in the ranges 0–20 kVp and 15–50 kHz respectively. In a previous work, our research group evaluated the amount of free charges transported by the Actuator 3 (annular geometry) supplied with a voltage of 6 kV peak and a frequency of 31 kHz [12]. In the present work, Actuators 1 and 3 (both made with 2 mm thick PVC) have been supplied with a voltage of 8 kV peak at a frequency of 27 kHz. This couple voltage-frequency guarantees a stable, strong and homogeneous plasma fulfilling impedance matching requirements between power supply and DBD load. Despite the change in supplying conditions, it has been verified that, for Actuator 3, plasma appearance, average power, induced jet and transported charges are the same already reported in reference [12]. This is ascribable to similar plasma behaviour because of the same average power supplying the discharge and the limited variation both for voltage and frequency [26]. By supplying Actuators 1 and 3 in the same way, it is possible to verify the influence of the actuator geometry solely, with respect to the amount of the free charges transported by the ionic wind onto a target surface. Actuator 2, with Teflon, has been used to increase the plasma extension and charge particles amount. In order to produce a homogeneous and stable discharge in Actuator 2, a sinusoidal voltage of 14 kV peak at a frequency of 36 kHz was used. The change of supply voltage and frequency is due to the actuator thickness and matching impedance requirements. As reported in Ref. [24], an increment of the applied voltage, by leaving unchanged discharge average power and induced flow, increases the amount of charged particles deposited onto the target surface.

The high voltage applied to the electrodes has been measured by means of a Tektronix P6015 capacitively compensated high voltage probe with a bandwidth up to 75 MHz. Charge flowing through the actuator has been evaluated by measuring the voltage across a 10 nF capacitor (Cm in Figure 3) connected between the buried electrode and the ground terminal. The voltage was detected by a Yokogawa low voltage probe with a 75 MHz bandwidth. A Tektronix TCP312 Hall current probe with a bandwidth up to 100 MHz has been utilized to detect the electrical current. This quantity was used to determine the ignition instant of the discharge, corresponding to the appearance of current streamers. All signals were acquired by a Yokogawa DL1740 4-channel, 500 MHz bandwidth, and 1 GS s−1 oscilloscope. The average power delivered to the discharge has been subsequently evaluated by means of the Lissajous figure [27], utilizing supplying high voltage and total charge flowing through the plasma. The power value is 6.8 W for the Actuator 1 and 18 W for the Actuator 2, with a standard deviation error of the 6%.

Charge distribution has been obtained from surface potential measurements by means of the numerical approach described in [25]. A plexiglass target was placed at a distance of 1 cm from the actuator end (in the x-direction in Figure 3) perpendicularly to the actuator dielectric slab. When Actuator 3 was used, dielectric surface was placed parallel to the target surface, at a distance of 1 cm, with the PSJA producing a jet hitting the target surface itself. The potential distribution induced by the free charges transported by the flow and deposited on the target were measured by means of a 341B 20 kV TREK electrostatic voltmeter. The zero position in the y-direction corresponds to intersection of the ionic wind jet axis in x-direction with the target surface. The electrostatic voltage probe scans the target in the y-direction. In Figure 3, the y-direction is positive on the right side. A second series of experiments has been performed by placing a stainless-steel grid at a distance of 1 mm far from the actuator (in the ‘x’ direction in Figure 3) to stop the free charges transported by the flow, when it was required. The tests have been repeated with the mesh connected to the ground, switch position 0-2 in the Figure 3, and with the mesh floating, switch position 0-1. The grid is a square with a 100 cm^2 size. The mesh of it had a 2 x 1 mm^2 rectangular holes and a 0.3 mm thick wire.

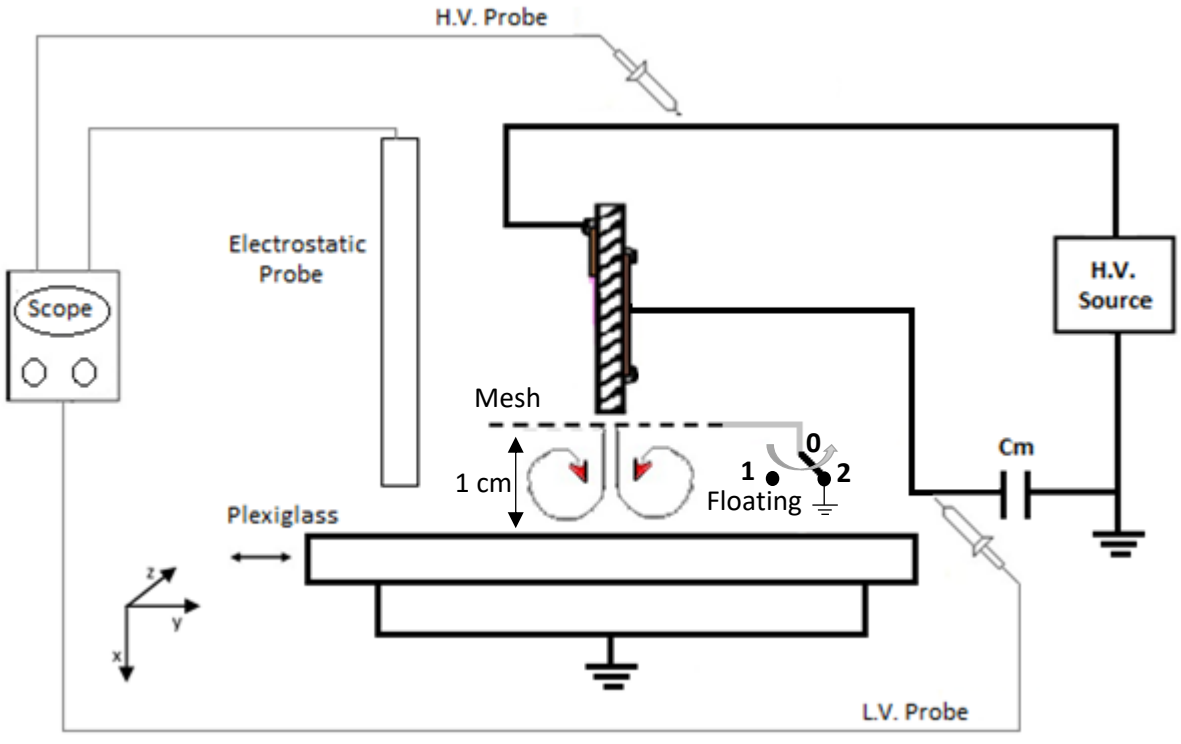

Figure 3. *Scheme of the experimental set-up.*

The tests have been performed in open air, with a temperature of 20 °C ± 1 °C, and humidity of 50% ± 5%. The experimental procedure, used to measure surface potential distribution, is performed through the following steps.

1. The Plexiglass surface was wiped by using a wet rag and then heated for 10 s with a hot gun to eliminate possible traces of humidity.
2. The electrostatic probe was moved over the Plexiglass surface checking the presence of a zero-voltage signal. If the zero condition was not achieved, step1 was repeated.
3. Discharge was ignited for a defined time interval. After switching off the discharge, the electrostatic probe was immediately moved over the Plexiglass plate, in the region where the induced jet hits the surface. Induced potential signal was acquired.

The velocity profiles along the x-direction were measured by means of a glass Pitot tube moved by a step motor with a 0.03 mm linear resolution. The Pitot tube (outer diameter of 1mm) was connected to a DCAL401 Sursense ultra-low pressure sensor with a 32 mV/Pa resolution [28]. The measurements were averaged over five tests, leading to a standard deviation error of the 5%. Schlieren diagnostic was used to visualize the induced hot flow produced by the plasma actuators. A Z-type configuration has been used [29] [30] with the light beam in the z-direction of Figure 3.

3. Results and discussion

The fluid dynamic behaviours of Actuators 1 and 2 were firstly analysed by means of the Schlieren technique to determine the influence of the dielectric thickness on the ionic wind distribution. The speed of the induced wind was measured by means of the Pitot tube. After these tests, the distribution of the surface potential on the target was measured and the performance of the actuators regarding the production and delivery of the charged particles was evaluated.

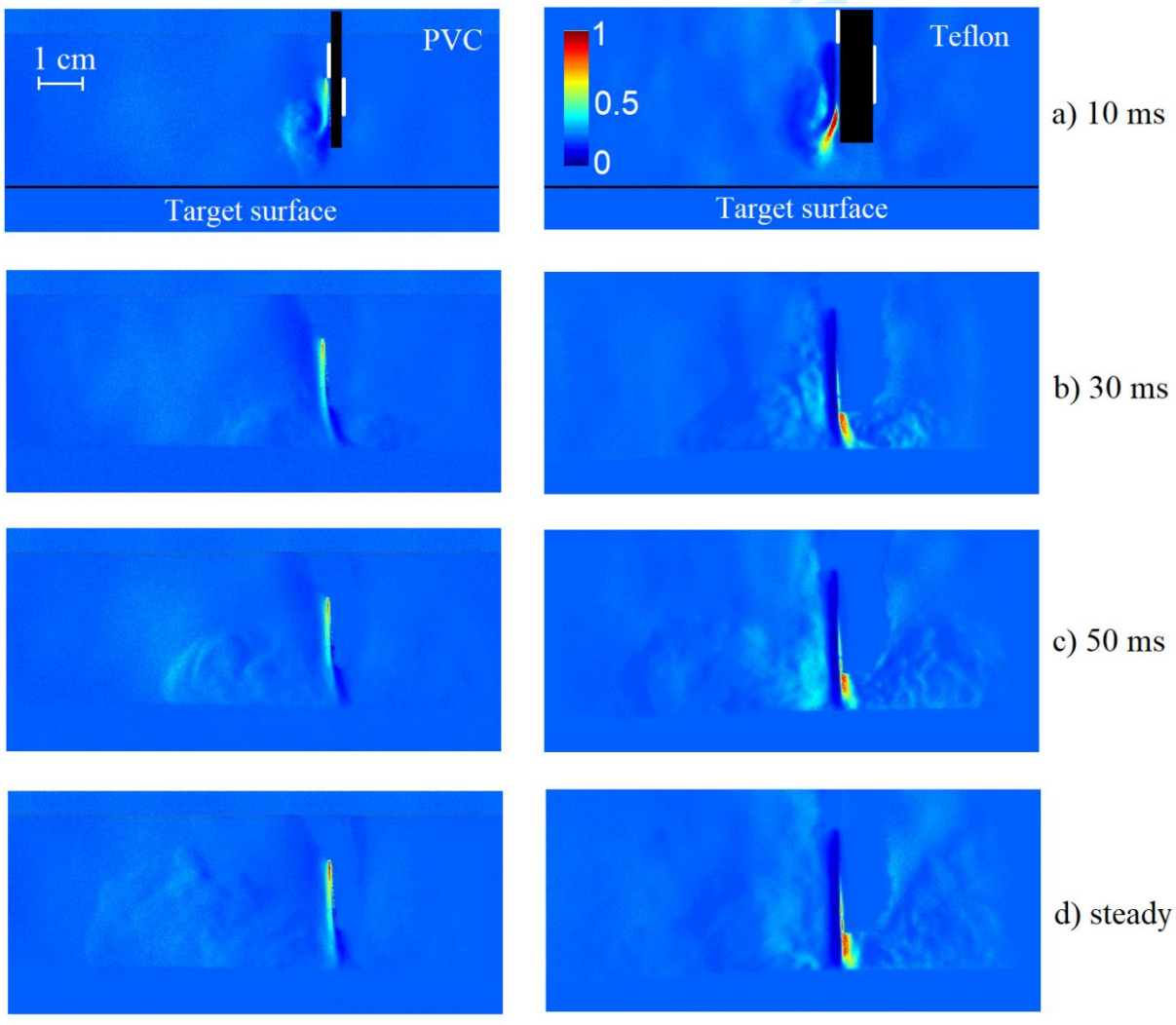

Figure 4. *Schlieren images of the induced jets generated by Actuator 1 (left images), and Actuator 2 (right images) after 10, 30, 50 ms from the discharge ignition and for the steady state operation.*

In Figure 4, a comparison of the Schlieren images acquired at different times after the discharge ignition is reported both for Actuators 1 (left hand side) and Actuator 2 (right hand side). In the first images of both actuators, the dielectric slab is highlighted in black, and the two copper electrodes in white. The horizontal black line represents the target surface. In the first picture of Actuator 2, a colormap representing the light intensity in per unit is highlighted. The distance between the actuator lower edge and the target surface is 10 mm. Hence the distance between the plasma end and the target is about 20 mm. The same distance was used to obtain the results reported in the investigation described in reference [23] where Actuator 3 (annular geometry) was tested.

Figure 4 shows the induced jet following the discharge ignition. After 10 ms the tangential jet propagates in the x-direction (the reference system is shown in Figure 1) producing a vortex against the stationary gas in front of the target. After 15 ms, it hits the target surface and starts to spread over the it. The two actuators produce quite similar induced jets. However, the speed of Actuator 2 (Teflon dielectric) is higher. This behaviour is highlighted by a wider diffusion region of the jet of Actuator 2 on the target surface. For both actuators, the jet does not diffuse symmetrically in the y-direction. The jet propagation is enhanced on the left side (i.e. the side of the negative y-direction Figure 3).

For both actuators, the induced jet velocity at zero height (onto the dielectric surface) was measured for three different distances from the end of the discharge along x-direction (Figure 3). As already mentioned, standard deviation for all measurements is within the 5%. The position at x = 0 corresponds to the end of the discharge, paying attention the Pitot tube does not touch the plasma end, avoiding discharge perturbation. The second position at x = 1 cm is located immediately beyond the actuator's edge. The last position is placed 1 cm away from the actuator lower edge, and thus at 2 cm from the end of the plasma discharge (where the target is usually placed). The plots in Figure 5 show that the Actuator 2 produces an induced wind velocity that is about the 50% higher than Actuator 1 at the discharge end. This difference is roughly maintained for all measurement positions. Higher velocity produced by Actuator 2 can be ascribed to a longer plasma extension (x-direction of in Figure 1) obtained by increasing the applied voltage and as a consequence higher average power feeding the discharge generated by this actuator [26][31][32].

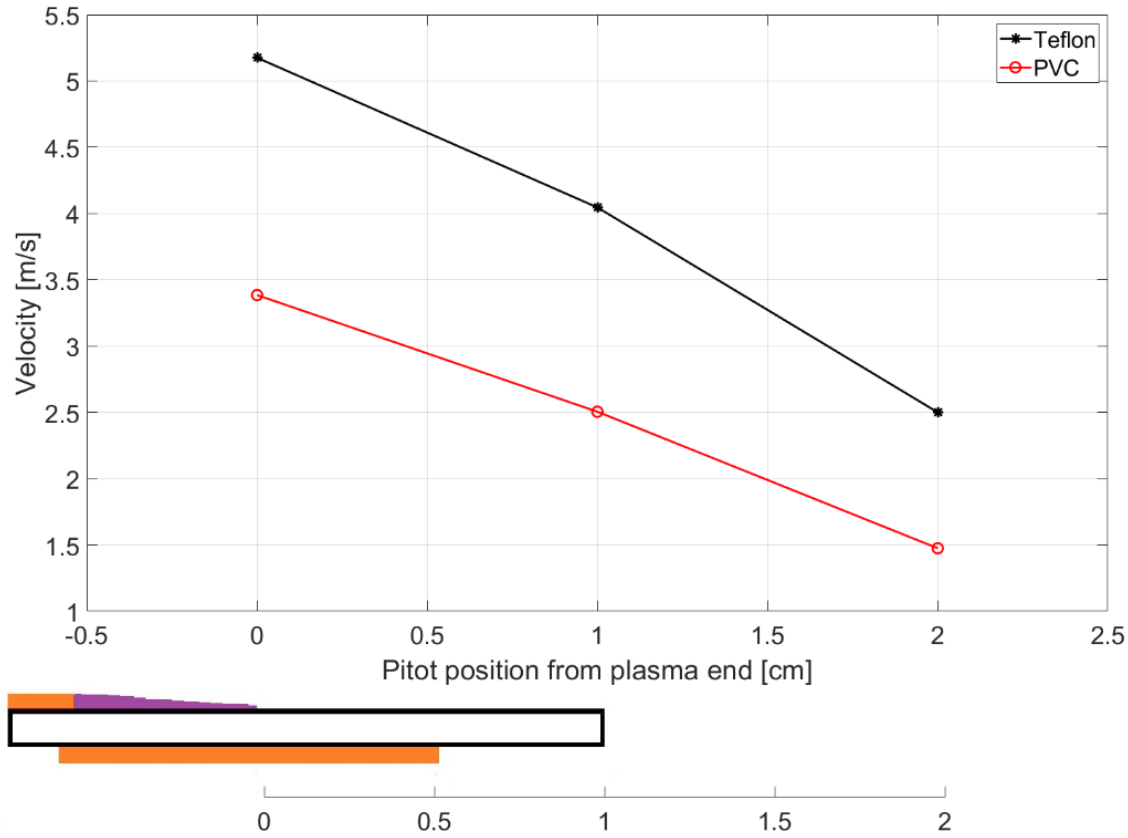

Figure 5. *Jet wind velocity at a distance of 0, 1, and 2 cm from the end of the plasma discharge for the Actuator 1 (red circles) and Actuator 2 (black stars).*

In order to see which electrode configuration is best suited to increase the charged particles deposition on a target surface, the flow velocity distribution in the cross-section of the jet at 2 cm in x-direction from the end of the plasma discharge (Figure 6.a) was measured for all actuators. These velocity profiles are useful to observe different fluid-dynamic behaviours of the three actuators. The velocity distributions were compared with the surface potential distribution on the target surface measured at the same distance from the end of the plasma discharge, after 10 seconds of discharge on (Figure 6.b).

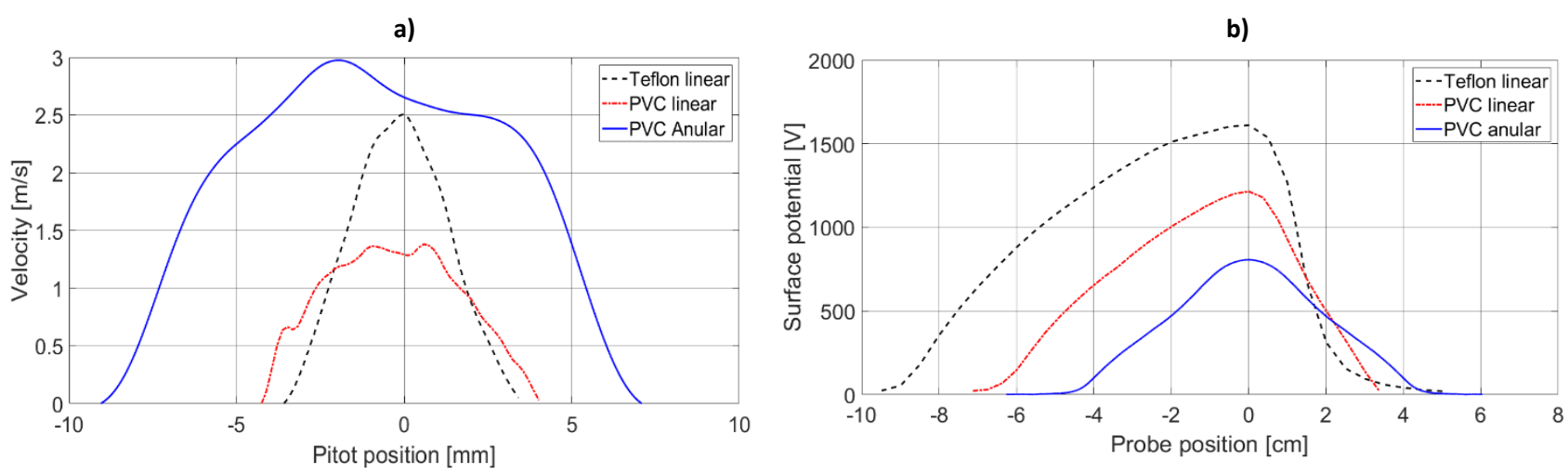

Figure 6. *Velocity profiles at 2 cm from the end of the plasma discharge on the left-hand side (a), surface potential distribution measured at the same distance, for 10 seconds of plasma switching on the right-hand side (b), for the three actuators.*

Actuator 3 produces a tubular jet characterized by an axisymmetric geometry, inducing a faster jet with a wider profile than those of the linear actuators. The charged particles are also deposited symmetrically around the jet axis with a 'bell' shaped distribution. On the contrary, when considering the potential induced by the charge particles deposited on the target surface (Figure 6.b), the profile of the linear actuators (Actuators 1 and 2) is broader than that of annular one (Actuator 3). Potential distribution profile for linear actuators is not symmetric with respect the axis normal to the target surface (x-direction in Figure 3). A higher amount of charges are deposited toward negative values of the y-axis (Figure 3). This is in agreement with Schlieren images reported in Figure 4, displaying, for both linear actuators, that induced jet does not diffuse symmetrically onto the target surface. The jet propagation is enhanced on the negative y-direction side (left hand side in the figure) with respect positive y-direction. Moreover, the maximum values of the potential obtained by the linear actuators largely exceed the values induced by the annular one. For Actuator 1 the potential is 50% higher with respect Actuator 3, going from a maximum of 800 V to 1200 V. This increase was obtained by modifying the actuator geometry solely, since materials and electrical quantities in the Actuators 1 and 3 were the same. As a matter of fact, the interaction of the tangential jets induced in Actuator 3, which merge and produce the perpendicular jet, favours the recombination of charged particles. Therefore, a reduced quantity of charges is deposited on the surface of the target, despite a higher ionic wind velocity. In Actuator 2, the maximum values of the induced potential undergo a further increase of about 400 V, reaching 1600 V, two times of that of Actuator 3. The increase of the distribution and the number of charges when passing from Actuator 1 to

Actuator 2 was obtained by increasing both dielectric thickness and supply voltage. Therefore, in test cases considered in this work, a strong increment in the amount of charged particles transported by a plasma actuator can be obtained by modifying both actuator geometry and supply conditions.

The distribution of the surface potential for different time intervals in which the plasma is on, in Actuators 1 and 2, is shown in Figure 7. The potential distribution and the resulting charge density had been performed in tests at the same room temperature (20° C) and humidity (45%) of the experiments of Ref. [24] and [25]. The potential distribution values and extension increase by increasing the time for which the plasma is on. This result is in agreement with the Schlieren images shown in Figure 4. In these pictures, incoming jet hits the surface after about 15-25 ms after the discharge ignition. Subsequently the jet spreads over the target surface, propagating for several centimetres away from the jet core itself. For longer plasma on-times, the swipe action of the jet onto target surface takes place for a longer time, leading to a more pronounced charge build-up. For Actuator 2 charge build-up takes place in a shorter time. After a plasma on-time of 250 ms, the maximum value of the induced potential is 1 kV, about 60 % of the final regime value. For Actuator 1, after the same time of plasma on, only a third of the regime value is achieved. This behaviour is due to the faster jet produced by Actuator 2 and the higher number of free charged particles generated by this actuator.

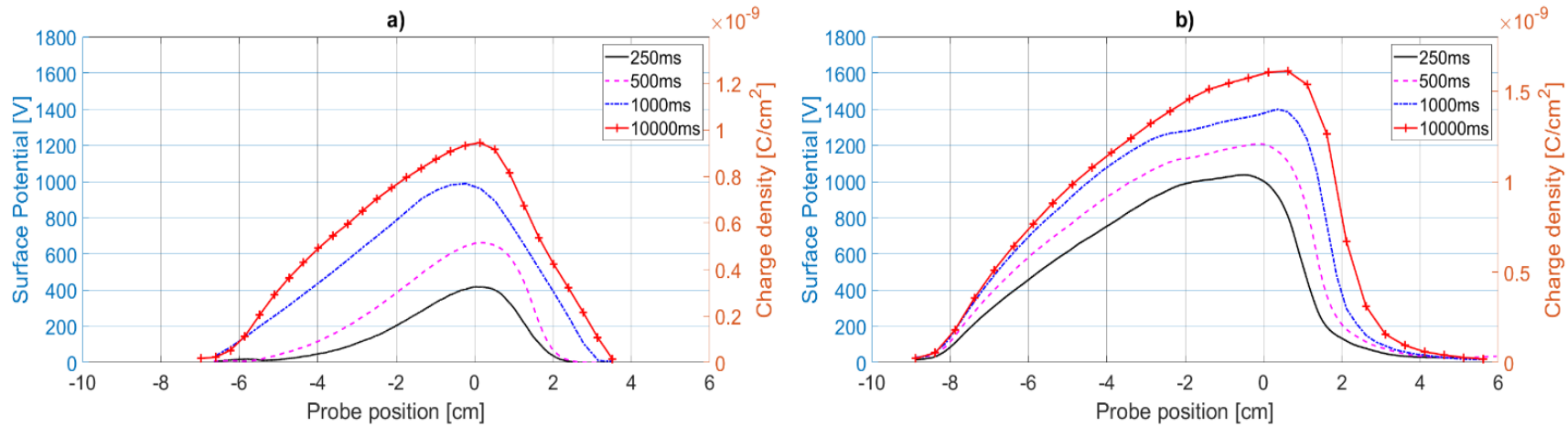

Figure 7. *Surface potential distribution measured by different time for which the plasma is on. for Actuator 1 (a), and Actuator 2 (b).*

A second series of surface potential measurements had been performed with a wire mesh inserted between the actuator and the target surface. These experiments have been performed to further increase the total amount of free charges reaching the target. As far as Actuator 2 presents the highest quantity of charged particles transported toward the target, results with this actuator solely will be presented. As it is shown in Figure 3, the mesh can be left floating or grounded. This had been done to see the behaviour of free charges, some of which is stopped by the wire mesh and the rest reach the target surface. In accordance with the Ref. [23], the charge distribution is modified when the wire mesh is present, or it is not, and when it is floating, or it is grounded. In Figure8.a the potential distribution on the target surface is shown. In the figure, the continuous blue line refers to the potential when the grid is not present, the black dashed line refers to the floating grid case, and the red line refers to the case without the grounded mesh case.

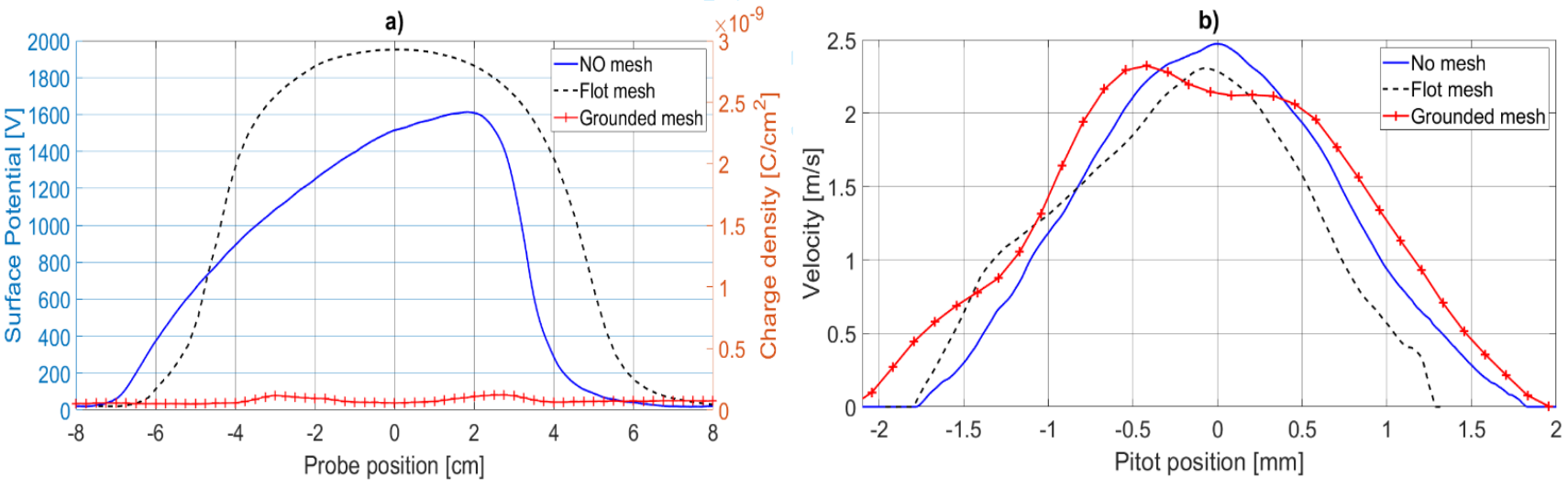

Figure 8. *Surface potential distribution obtained by Actuator 2, measured on the target slab with grounded grid (red line), without grid (blue continues line), and with floating grid (black dashed line), on the left-hand side (a). Velocity profiles measured at the same conditions and position, on the right-hand side (b).*

When the wire mesh is connected to ground (red line), about 95 % of the charges inside the flow are conveyed by means of the mesh to ground, severely limiting the number of charge particles that reach the target surface. Unlike what was previously seen in Ref [23], in Actuator 2 the distribution of the surface potential increases by the 25 % when the grid is left floating, compared with the potential measured without grid. A possible explanation for this increment, is a different fluid-dynamic regime for the two conditions. Figure 8.b shows the velocity profiles, measured by the Pitot tube, at 2 cm from the end of the discharge (without the target) without the wire mesh (blue continues line) and with the grounded wire mesh grounded (red line), or left floating (black dashed line). By considering a standard deviation error of the 5%, the differences of the three velocity profiles are very limited. Therefore, the increase in the potential induced on the target surface when the floating grid is used, is not strictly related to the variation of the induced flow with and without the wire mesh. This increase is due to the different interaction between electrodynamics and fluid dynamics, in the two cases. The floating wire mesh is an equipotential plane orthogonal to the flow direction. Therefore, the electrodynamics on this region is changed and, as a consequence, its interaction with the fluid dynamics is different. This physical explanation will be investigated in the last part of the paper, by utilizing electrostatic simulations.

In Figure 9 the surface potential distribution for different time intervals with the floating wire mesh (Figure 9.a), is compared with that without mesh (as in Figure 9.b).

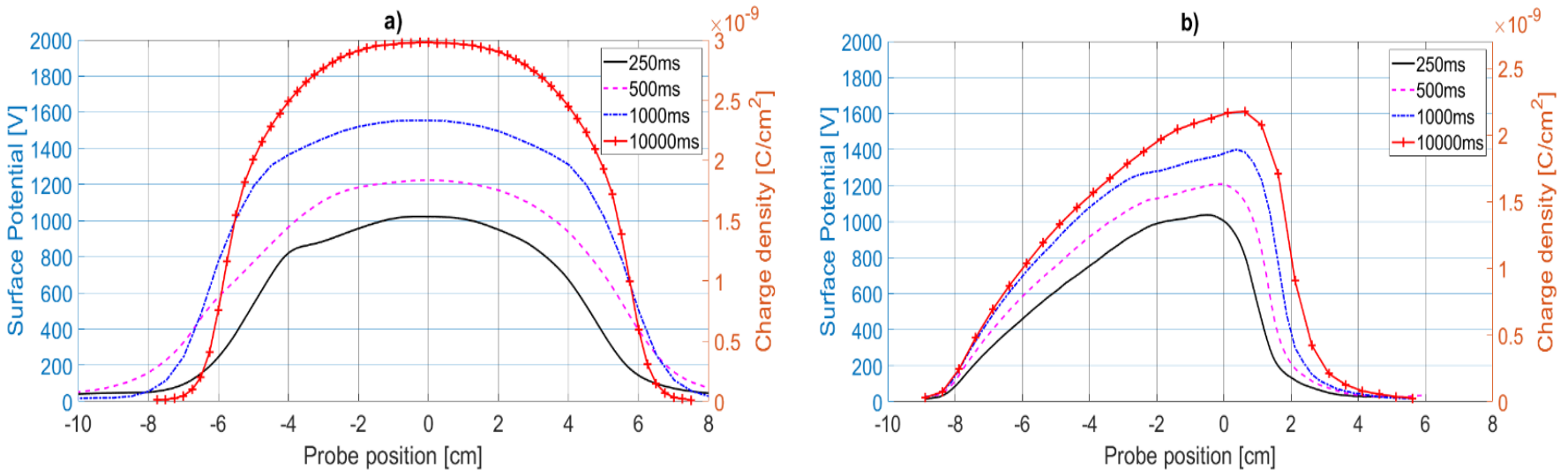

Figure 9. *Surface potential distribution for Actuator 2, measured by increasing plasma on time, with floating mesh on the left (a), and without mesh on the right (b).*

When the floating mesh is present, the potential distribution becomes symmetric and the potential values increase. This also is due to the equipotential plane of the mesh that leads to a symmetric potential distribution on the target surface on the side of the flow. The difference of the maximum values of the potential when the floating mesh is present, becomes larger when the time ignition of the plasma increases. This behaviour is clearly visible in in Figure.a. The maximum potential value as a function of plasma-on time is displayed here, with (red crosses) and without floating mesh (black circles). In the first 500 ms, the maximum values are nearly equal for both cases. For a further increase of the time from the discharge ignition, when the floating mesh is used, higher induced potentials are measured. At this time a higher potential of the wire mesh is detected as shown in Figure.b. Here the potential of the wire mesh as a function of time after the discharge ignition is shown. The time zero corresponds to the discharge ignition (detected with the Hall current probe). After about 10 ms the mesh potential starts to increase as the induced jet approaches it surface. After approximately 500 ms the mesh potential reaches a value of around 1900 V, and further increases up to 2000 V after 10 s. The final potential of the floating mesh is the same measured on the target surface. Despite this, the charge deposition dynamics on the target surface is slower than the mesh charging mechanism. This is due to the time needed for free charges to reach the target surface after overcoming the potential barrier generated by charges that have already reached the surface itself.

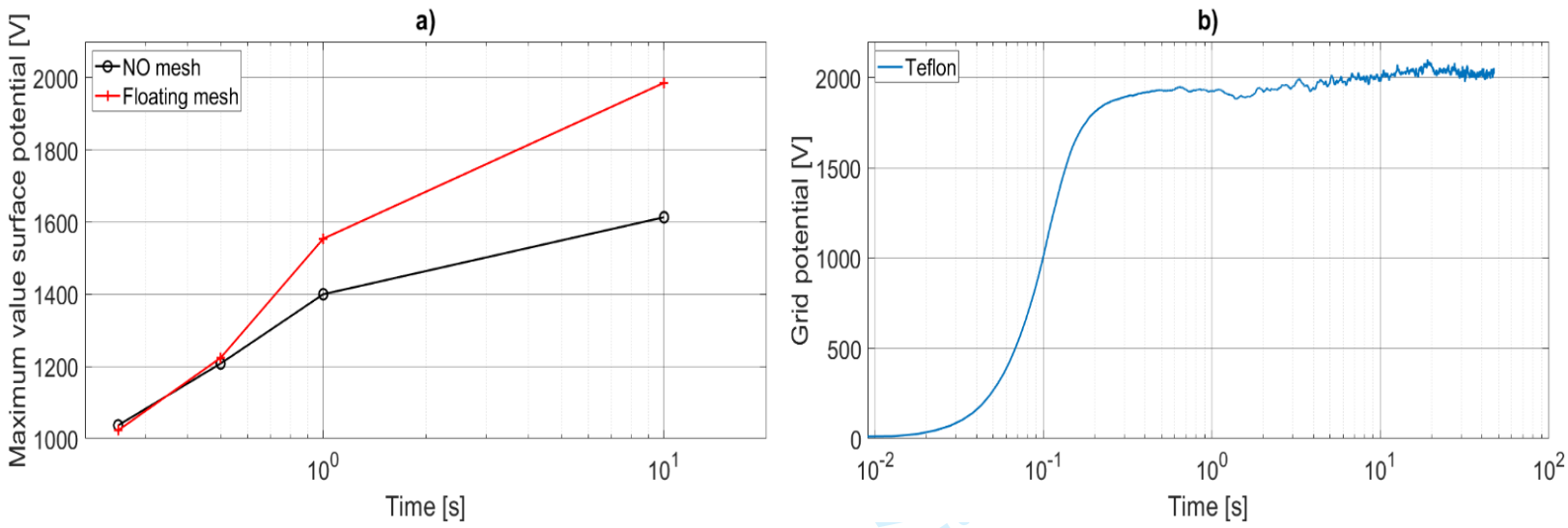

Figure 10. *Maximum potential values on the target surface for different time intervals with the plasma on when the floating wire mesh is present on the left side of the figure (Figure 9.a) and potential of the wire mesh as a function of the plasma-on time, on the right side (Figure 9.b).*

In order to obtain an insight on the mechanisms by which the electric field affects the transport of electric charges by the jet, a 2D finite element analysis was carried out. The Ansoft Maxwell 2D electrostatic solver was utilised to evaluate the distribution of the electric field in the region of interest. The experimental results (i.e., the applied voltage and the deposited charge) have been used as inputs of the analysis. In Figure 11, the calculation domain for the two linear actuators described in this paper are shown. The contour plots shown here refer to a condition in which the powered electrode is set to the potential equal to the amplitude of the sinusoidal supply voltage (i.e., 8 kV for Actuator 1, and 14 kV for Actuator 2). The electric field distribution provides information about the forces acting on the charges transported by the flow in the region away from the electrode.

In Figure 12, the distribution of the x-component of the electric field E_x along the line Γ running from the powered electrode to the target is shown for Actuator 1. The positioning of the curve Γ for Actuator 1 is shown in Figure 11.a. Using the reference system in Figure 3, a positive electric field E_x is directed toward the target. In this analysis the lower edge of the actuator dielectric slab is located at x = 15 mm on the line Γ. The region between 15 and 25 mm represents the airgap between the actuator and the target.

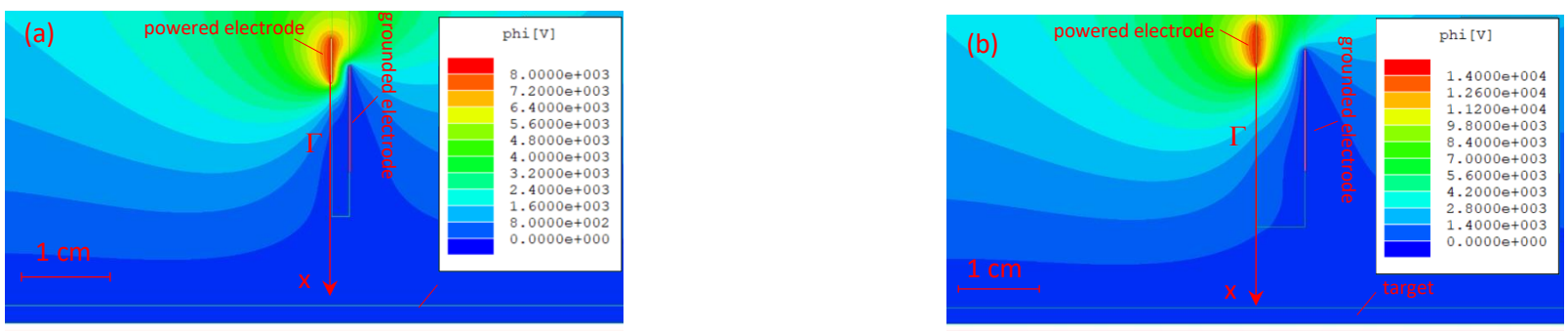

Figure 11. *Electric potential contour plot for Actuator 1 (a) and Actuator 2 (b).*

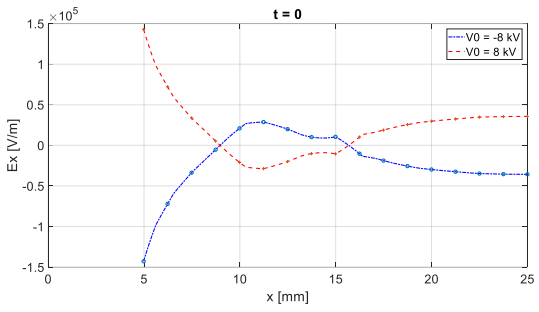

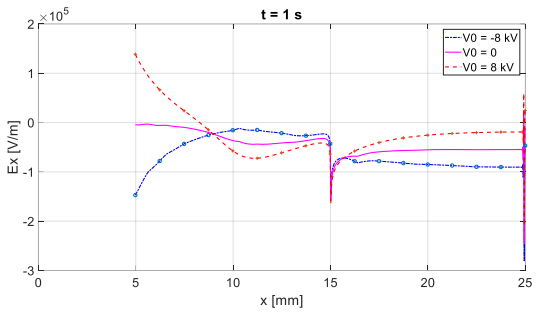

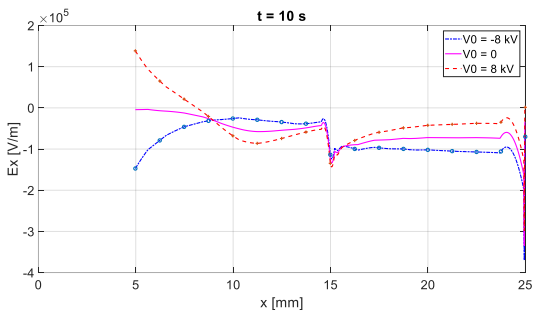

Figure 12. *Distribution of the x component of the electric field along Γ for Actuator 1.*

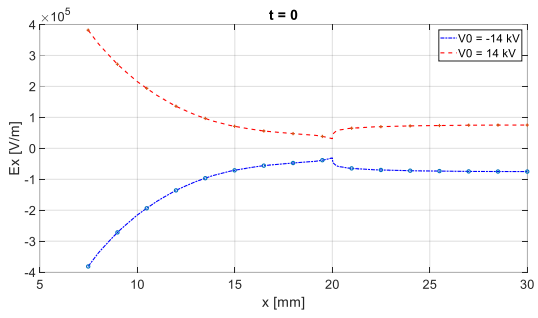

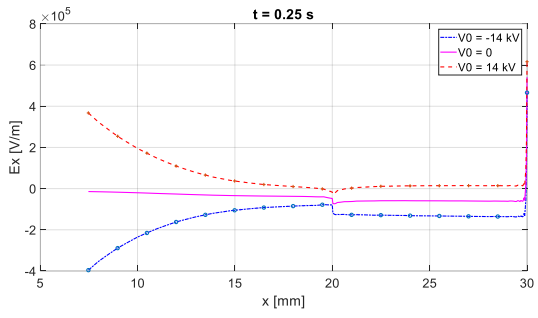

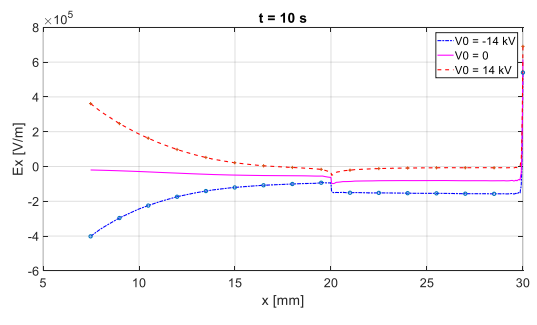

Figure 13. *Distribution of the x component of the electric field along Γ for Actuator 2.*

The results have been calculated at different times after the actuator switch-on, taking into account of the contribution of the deposited electric charge. Since the applied voltage V_0 varies sinusoidally, the electric field E_x is plotted for V_0 = -8kV, V_0 = 0 and V_0 = 8kV. It is worth noting that the characteristic time variation of the deposited charges is much higher than the period of the electric supply system. As a result, the deposited charge is assumed to be constant over a single supply system period. The electric field produced solely by the deposited charge is represented by the plot for V_0 = 0. As can be observed in Figure 12, the electric field in the airgap region is relatively low at t = 0, and varies between 35 and -35 kV m^{-1}. While the electric charge settles on the target surface over time, an adverse field is formed, which exerts a repulsive force on ions. At t = 1 s, on the target the electric field is negative for the entire cycle duration, with an average value of about - 45 kV m^{-1}. Despite of this, the charge build-up continues. In this phase, the jet produced by the actuator is responsible for a convective ion flux which prevails on diffusion flux due to the adverse electric field. After an approximately 10 s switch on time, an equilibrium condition is eventually reached, as the charge build-up produces an electric field that is sufficient to compensate the incoming convection ion flux on the target wall. The distribution of the resulting charge surface density on the target depends on the fluid dynamic behaviour of the jet, as well as on the local dynamics by which the charge deposit is formed. A similar behaviour can be observed on Figure 13 for Actuator 2. Here, the actuator lower edge is located at x = 20 mm, and the airgap region between the actuator and the target is between 20 and 30 mm. In this case too, an adverse field is formed in the airgap region between the actuator and the target due to the deposited charges. E_x is observed to assume negative values for almost the whole supply system period at t = 250 ms. Nevertheless, the positive charge continues to cumulate up to t = 10 s, when an equilibrium condition is reached.

When a floating wire mesh is utilised, the numerical analysis shows a significant change in the distribution of the electric field. As can be observed in Figure , one of the most remarkable effects produced by the mesh is the creation of a vast region downstream of the mesh itself in which the distribution of the electric field is fairly uniform and substantially independent of the applied voltage.

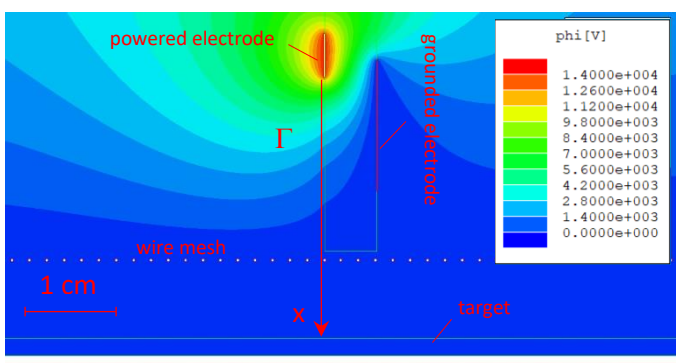

Figure 14. *Electric potential contour plot for Actuator 2. Powered electrode voltage is set to 14 kV, mesh voltage is set to 0.*

Figure reports the distribution of the x-component of the electric field E_x along the line Γ running from the powered electrode of Actuator 2 to the target with the floating mesh. The positioning of the curve Γ is shown in Figure 14. As the jet produced by the actuator hit the mesh, it begins to acquire a positive potential. Initially, the positive potential is acquired mainly due to the electrons that are lost in the recombination of the ions. At the same time, the positive potential is acquired by the target, too. However, the rate at which the charge deposited on the target is lower than the rate at which the charges and the potential of the mesh increases. As a result, a positive E_x develops in the region between the mesh and the target. Since the mesh potential and the deposited charge weakly depend on the sinusoidal applied voltage, the electric field is roughly constant during the supply system period. Its time behaviour is governed by the loading dynamics of the mesh and the target. An adverse field region is observed to form before the jet hit the mesh. As shown in Figure 15, the E_x field is negative during the entire electric supply period in the region between x = 15 mm and the mesh for at t = 0.25 s. Also, in this case, ion convection dominates over the repulsive electric force. Despite the adverse electric field reaches a value of - 125 kV m^{-1}, an ion flux is delivered past the mesh. In this region the E_x electric field becomes positive and is distributed in the whole width between the mesh and the target. Therefore, it promotes a uniform charge deposition. The equilibrium condition is reached when the potential acquired by the target due to the deposited charges equals that of the wire mesh. In this condition, the electric field in the region past the wire mesh, and -consequently- the ion drift due to the electric field toward the target, assume an almost zero value (see Figure 15, t = 10 s) . At the same time, the adverse field in the region upstream the mesh is sufficient to inhibit the ion flux.

Figure 15. *Distribution of the x component of the electric field along Γ for Actuator 2 with a floating mesh.*

4. Conclusion

In this paper, a comparison was carried out between two types of linear DBD actuators, made of PVC and Teflon respectively. The comparison was focused on the fluid dynamic regime of the jet produced by the actuators and on the effectiveness with which the electric free charges carried by the jet are deposited on a target. This last aspect is of particular interest since recent publications have reported that the amount of deposited charges is related to the biocidal efficacy of the device. The electric charge deposited on the target has been measured by means of an electrostatic voltmeter. Fluid dynamic investigations have consisted of Schlieren flow visualizations and a flow velocity measurement by means of Pitot probes. It was observed that the maximum jet velocity produced by Actuator 2 is approximately two times higher than the maximum velocity for Actuator 1. As a consequence, Actuator 2 is capable of depositing a higher amount of electric charges on the target. A comparison between the performances of the linear actuators investigated in this work and the analogous experimental results observed for an annular actuator has revealed that linear actuators produce a wider profile of the deposited charge and higher maximum values. The results show that it is possible to strongly increase the number of charged particles transported by a plasma actuator by modifying actuator geometry and supply conditions.

A second set of experiments had been carried out introducing a wire mesh between the actuator and the target surface, trying to further increase the number of deposited charges onto the target surface. The mesh does not significantly affect jet fluid dynamics, but electric field distribution solely. The presence of a grounded mesh almost completely neutralizes the positive charges in the jet, substantially reducing the charge build up on the target. When the mesh is floating, the charge deposition is enhanced and the surface of the target where the charges are deposited is larger than those obtained by linear actuators without mesh. A numerical investigation revealed that, in this condition, a region is created between the mesh and the target where the electric field promote a higher and more uniform charge deposition.

References

[1] Santhanakrishnan A and Jamey D J 2007 Flow control wit plasma synthetic jet actuators *J. Phys. D: Appl. Phys*. **40** 637.

[2] Neretti G, Seri P, Taglioli M, Shaw A, Iza F and Borghi C A 2017 Geometry optimization of linear and annular plasma synthetic jet actuators. *J. Phys. D: Appl. Phys*. **50**

[3] N. Bénard, J. Jolibois, E. Moreau, R. Sosa, G. Artana, and G. Touchard. Aerodynamic plasma actuators: A directional micro-jet device. J Thin Solid Films. 2008; 516; 6660-6667. DOI: 10.1016/j.tsf.2007.11.039.

[4] S.H. Kim,W. Hong, and C. Kim. Separation Control Mechanism of Airfoil Using Synthetic Jet. J. Mechanical Science and Technology. 2007; 21, 1367-1375.

[5] Moreau E 2007 Airflow control by non-thermal plasma actuators *J. Phys. D: Appl. Phys*. **40** 605–36

[6] Borghi C A, Carraro M R, Cristofolini A, and Neretti G 2008 Electrohydrodynamic interaction induced by a dielectric barrier discharge. *J. Appl. Phys* **103** 063304

[7] Fridman A, Kennedy L A, 2004 Plasma Physics and Engineering (Boca Raton, FL: CRC Press)

[8] Fridman A, Chirokov A, and Gutsol A. 2005 Non-thermal atmospheric pressure discharges. *J. Phys. D: Appl. Phys.* **38** (2)

[9] Fridman G, Brooks A.D., Balasubramanian M., Fridman A., Gutsol A., Vasilets V. N., Ayan H., Friedman G. 2007 Comparison of direct and indirect effects of non-thermal atmospheric-pressure plasma on bacteria. *Plasma Process. Polym.* **4** 370–5.

[10] Elena Sysolyatina , Role of the Charged Particles in Bacteria Inactivation by Plasma of a Positive and Negative Corona in Ambient AirPlasma Processes and Polymers 11(4), DOI: 10.1002/ppap.201300041

[11] Borghi C A, Carraro M R, Cristofolini A, and Neretti G 2008. Electrohydrodynamic interaction induced by a dielectric barrier discharge. *J. Appl. Phys* **103** 063304.

[12] Neretti G, Ricchiuto A C and Borghi C A 2018 Measurement of the charge distribution deposited by an annular plasma synthetic jet actuator over a target surface. *J. Phys. D: Appl. Phys.* **51**.

[13] Taglioli M, Shaw A, Wright A, FitzPatrick B, Neretti G, Seri P, Borghi C A and Iza F 2016 EHD-driven mass transport enhancement in surface dielectric barrier discharges. *Plasma Sources Science and Technology* **25**.

[14] A. Fridman, 'Plasma Chemistry', Cambridge University Press, 2012, ISBN: 978-1107684935.

[15] Laroussi 2005 Low Temperature Plasma-Based Sterilization: Overview and State-of-the-Art *Plasma Processes and Polymers* **2**(5)

[16] Akishev Y, Machala Z, Koval N, 2019 Special issue on recent developments in plasma sources and new plasma regimes. *J. Phys. D: Appl. Phys*. **52** 130301.

[17] Giardina A, Tampieri F, Biondo O, Marotta E, Paradisi C, 2019 Air non-thermal plasma treatment of the herbicides mesotrione and metolachlor in water. *Chemical Engineering Journal* **372** 171-180.

[18] Zhang Y, Wei L, Liang X, Šimek M, 2019 Ozone Production in Coaxial DBD Using an Amplitude-Modulated AC Power Supply in Air. *Ozone: Science and Engineering* **41**(5) 437-447.

[19] F Tampieri, A Giardina, FJ Bosi, A Pavanello, E Marotta, B Zaniol, G. Neretti, C. Paradisi, Removal of persistent organic pollutants from water using a newly developed atmospheric plasma reactor *Plasma Processes and Polymers* **15** (6), 1700207.

[20] Fridman G, Friedman G, Gutsol A et al 2007 Applied plasma medicine Plasma Process. Polym. **5** 503–33

[21] Neretti G, Morandi B, Taglioli M, Poglayen G, Galuppi R, Tosi G and Borghi C A 2018 Inactivation of Eimeria oocysts in aqueous solution by a dielectric barrier discharge plasma in contact with liquid. *J. Plasma Med*. **8** 155–62.

[22] Yiguang J, Wenting S 2015 Plasma assisted combustion: Dynamics and chemistry. *Progress in Energy and Combustion Science*. **48** 21-83.

[23] Neretti G, Ricchiuto A. C, Galuppi R, Poglayen G, Morandi B, Marotta E, Paradisi C, Tampieri F, Borghi C. A 2018 Indirect Inactivation of *Candida guilliermondii* by Using a Plasma Synthetic Jet Actuator: Effect of Advected Charged Particles. *Plasma Medicine*. **8** 255-268.

[24] Ricchiuto A C, Borghi C A, Cristofolini A, Neretti G 2019 Measurement of the charge distribution deposited over a target surface by an annular plasma synthetic jet actuator: influence of humidity and electric field. *Journal of Electrostatics.* **107**

[25] Neretti G, Ricco M 2019 Self-Tuning High-Voltage and High-Frequency Sinusoidal Power Supply for Dielectric Barrier Discharge Plasma Generation. *Electronics*. **8** 1137.

[26] Neretti G, Cristofolini A, Borghi C A, Gurioli A, and Pertile R. 2012 Experimental results in DBD plasma actuators for air flow control. *IEEE Transactions on Plasma Science*, 40(6) 1678-1687

[27] Pon J, Moreau E and Touchard G 2005 Assymmetric surface dielectric barrier discharge in air at atmospheric pressure: electrical properties and induced airflow characteristics. *J. Phys. D: Appl. Phys*. **38** 3635–42.

[28] Cristofolini A et al 2012 Schlieren imaging in a dielectric barrier discharge actuator for airflow control. *J. Appl. Phys*. **111** 033302.

[29] Neretti G, Cristofolini A and Borghi C A. 2014 Experimental investigation on a vectorized aerodynamic dielectric barrier discharge plasma actuator array. *J. Appl. Phys*. **115** 163304.

[30] Settles G S 2001 Schlieren and Shadograph Techniques (Berlin: Springer)

[31] Forte M, Jolibois J, Pons J, Moreau E, Touchard G, Cazalens M 2007 Optimization of a dielectric barrier discharge actuator by stationary and non-stationary measurements of the induced flow velocity: application to airflow control. *Exp Fluids* **43** 917-928

[32] Durscher R, Roy S 2012 Evaluation of thrust measurement techniques for dielectric barrier discharge actuators. Exp Fluids 53 1165-1176